01 Jan 2024

The Effect of Nanomorphology as Quantified Via the K-Index on the Drug Delivery Properties of Isocyanate-Derived Aerogels

Stephen Y. Owusu

A. B.M.Shaheen Ud Doulah

Vaibhav A. Edlabadkar

Kamden J. George

et. al. For a complete list of authors, see https://scholarsmine.mst.edu/chem_facwork/4021

Recommended Citation

S. Y. Owusu et al., "The Effect of Nanomorphology as Quantified Via the K-Index on the Drug Delivery Properties of Isocyanate-Derived Aerogels," *ACS Applied Polymer Materials*, American Chemical Society, Jan 2024.
The definitive version is available at https://doi.org/10.1021/acsapm.4c01765

ACS APPLIED POLYMER MATERIALS

pubs.acs.org/acsapm Article

The Effect of Nanomorphology as Quantified via the *K*-Index on the Drug Delivery Properties of Isocyanate-Derived Aerogels

Stephen Y. Owusu, A. B. M. Shaheen Ud Doulah, Vaibhav A. Edlabadkar, Kamden J. George, and Chariklia Sotiriou-Leventis*

Cite This: *ACS Appl. Polym. Mater.* 2024, 6, 10655−10668 Read Online

ACCESS | Metrics & More | Article Recommendations | Supporting Information

ABSTRACT: This study explores the potential to predict the drug-loading and release profiles of aerogels based on their morphologies: a milestone in drug delivery research, which can help save time and cost in formulating new aerogel drug carriers and cut-down evaluation of the drug delivery capabilities of aerogels to a few experimental runs. Polyurea (PUA) and poly(isocyanurate-urethane) (PIR-PUR) aerogels were used as model systems, while 5-fluorouracil (5-FU) and paracetamol (PM) were used as model drugs. These model systems were chosen because they can be synthesized into different morphologies, which can be quantified by the so-called *K*-index (water contact angle divided by porosity). The model drugs were loaded onto the aerogels using a physical adsorption method, and the drug-loaded aerogels were characterized with FT-IR, SEM, DSC, XPS, and UV spectroscopy. Our study revealed that drugs are loaded onto the surfaces of macropores, mesopores, or fibers depending on the morphology being studied and can be released quickly or slowly depending on the location of the drugs and different surface energies associated with different pore surfaces within the different morphologies onto which the drugs were loaded. Comparing all the morphologies studied, the various nanoparticle-based nanostructures (K = 1.2−1.5) and entangled nanofibers (K = 1.6) could uptake larger amounts of drug; fused nanoparticles (K = 1.5) and bicontinuous nanostructures (K = 2.2) are more suitable for fast-release formulations; morphologies with *K*-indexes equal to 1.2, 1.3, and 1.6 and those containing nanoparticles entangled with different ratios of nanofibers (K = 1.7−2.0) are more suitable for sustained-release formulations; and nanofibrous morphologies (K = 1.6) are more suitable for controlled-release formulations.

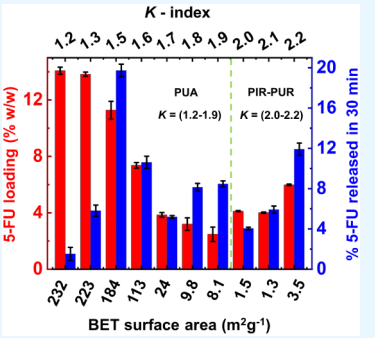

KEYWORDS: *aerogels, polyurea, polyurethane, morphology, drug delivery, 5-fluorouracil, paracetamol, Langmuir model, Freundlich model, Fickian diffusion, sustained release, controlled release*

1. INTRODUCTION

Drug delivery systems (DDSs) have received increased attention and proven to be better alternatives to conventional dosage forms due to their improved pharmacokinetic and pharmacodynamic properties.[1] The unique feature of DDSs, which enables them to achieve this goal, is their ability to load drugs to prevent their degradation and loss[2] and release the loaded drugs selectively to their site of action in a programmable (controlled release) or slow manner (sustained release).[3] This property of DDSs enables them to maintain therapeutic amounts of the drug at the target site, thereby reducing side effects associated with conventional drug delivery and improving drug efficacy.[4]

Aerogels are being extensively investigated as drug delivery platforms due to their unique low density,[5] high surface area,[6] and high porosity.[7] High porosity and surface area are highly desirable properties for drug delivery applications since they inhibit the crystallization of loaded drugs and contribute to their amorphization.[8] Amorphization of drugs within the porous network of aerogels increases the bioavailability of drugs since drugs have higher energy and dissolve more readily in their amorphous form compared to their crystalline form.[9] Loading drugs within the porous network of aerogels is also done to gain control over their drug release profiles, produce gastro-retentive dosage forms, and protect drugs from damaging external factors/conditions.[10]

High porosity and surface area in aerogels result from the assembly of 3-D networks of organic polymers, inorganic materials, or colloids of composites.[11] Different aerogels have distinct morphologies due to their 3-D network formation mechanism which happens mainly through the mode of the phase separation of the polymer during the sol−gel reaction.[7,12] Among the few aerogels that have been demonstrated to show varying morphologies depending on their formulation are polyurea (PUA) and poly(isocyanurate-

Received: June 11, 2024
Revised: August 9, 2024
Accepted: August 12, 2024
Published: August 27, 2024

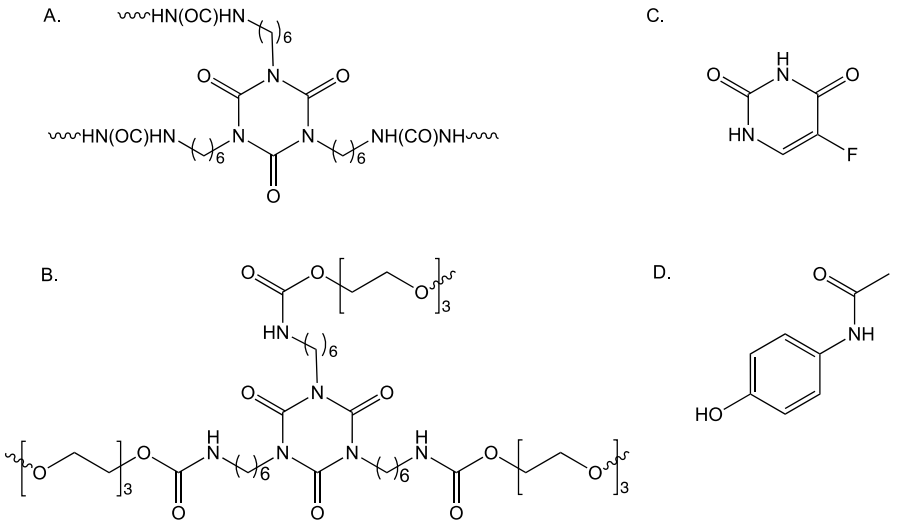

Figure 1. Structures of polyurea (PUA) (A), poly(isocyanurate-urethane) (PIR-PUR) (B), 5-fluorouracil (5-FU) (C), and paracetamol (PM) (D).

urethane) (PIR-PUR) aerogels whose structures are shown in Figure 1A,B, respectively.

Certain morphologies of PUA skeletal frameworks result from phase separation of solid nanoparticles in a random or ordered fashion, yielding randomly distributed or organized caterpillar-like nanoparticulate networks with various aspect ratios. However, if the developing polymer is phase-separated as an "oily" phase that gets solidified later, the morphology of the aerogel skeletal networks can be quite diverse, ranging from thin nanofilaments to small solid microspheres embedded in nanofibers, to larger solid microspheres with some fibers emanating from their surface.[13]

PIR-PUR aerogels made with the same aliphatic triisocyanate as the PUA aerogels reacting with short aliphatic diol derivatives of ethylene glycol also exhibit varying skeletal morphologies quite different from those in polyurea. These morphologies include small micrometer-sized spheroidal particles or fused microspheres. A unique morphology in these PIR-PUR aerogels, not observed in the corresponding polyurea aerogels, is a bicontinuous morphology in which the solid and porous networks are similar and can be considered to consist of large nanospheres fused at their necks. It was proposed that PIR-PUR morphologies are formed from the initial phase separation of an immiscible oily (i.e., liquid) mixture of oligomers followed by solidification as the polymerization process within the oily phase continues.[12,14] Due to difficulty in correlating the linguistic nomenclature of various morphologies to quantitative parameters to enhance their synthesis by design, morphologies obtained from different formulations of PUA and PIR-PUR aerogels have been described numerically using the *K*-index which is defined by eq 1[13]

$$K\text{-index} = \frac{\text{contact angle}(\theta)}{\text{porosity}(\Pi)} \quad (1)$$

The *K*-index is an empirical factor that quantifies our perception of two basic qualities of a nanostructure as seen in scanning electron microscopy (SEM), openness (via the porosity) and texture (via the contact angle of water droplets resting on the material), and corresponds to different morphologies of aerogels because different morphologies have different openness and texture. It was found empirically that the ratio of the quantifiers of openness (porosity) and of texture (contact angle) correlates uniquely with the morphology. This has been described in detail in our previous work.[13]

PUA aerogels used in this study have *K*-indexes from 1.2 to 1.9 corresponding to different morphologies ranging from caterpillar-like (1.2) or worm-like (1.3) assemblies of nanoparticles to fused nanoparticles (1.5) to cocoon-like nanostructures (1.7−1.8) and almost bald microspheres (1.9). PIR-PUR aerogels of this study have *K*-indexes 2.0−2.2 which correspond to fused spheres, spheroidal nanostructures, and bicontinuous nanostructures, respectively.

Morphologies of various materials including nanoparticles,[15] composites,[16] hydrogels,[17] and micelles[18] have been found to influence their drug release profiles. However, the effect of aerogel nanomorphologies on their drug-loading and release profiles is not reported. We took the challenge to explore this area by taking advantage of the several unique morphologies of PUA and PIR-PUR aerogels.[13,14] Interestingly, it is also reported that polyurea and polyurethane nanosystems can be biocompatible and biodegradable,[19−21] making their usage as drug delivery systems more promising and thereby contributing to the significance of this study.

Since drug loading and release is known to be influenced by the porosity of aerogel drug carriers,[22,23] ten samples, seven PUA, and three PIR-PUR aerogels with about the same porosities but different morphologies were selected for this study. Two model drugs have been selected for this study due to their different utility and different molecular structures. Specifically, 5-fluorouracil (5-FU) (Figure 1C) was selected as the model drug for all analysis discussed in this project partly due to its ubiquitous usage as an anticancer drug in drug delivery studies[24] and partly to its small molecular size, which is thought to lead to easy loading and release from drug carriers.[25] Paracetamol (PM) (Figure 1D) was selected partly because it is an analgesic and antipyretic agent which can also be used in combination therapy to relieve severe acute pain[26] and partly due to its lower solubility in the release medium (phosphate-buffered saline (PBS) solution at pH 7.4) compared to 5-FU, hence presenting different usage and solubility properties. Also, since PM has more functional groups (−OH, and −NH), which can form hydrogen bonds with PUA and PIR-PUR aerogels compared to 5-FU (only

https://doi.org/10.1021/acsapm.4c01765
ACS Appl. Polym. Mater. 2024, 6, 10655−10668

−NH), PM has a stronger affinity to the surface of the aerogels compared to 5-FU.

Aside from the quantitative drug-loading and release analysis of these samples, we considered various mathematical loading models (Langmuir and Freundlich isotherms)[27] and release models (zero-order, first-order, Higuchi, Korsmeyer−Peppas, and a sigmoidal equation with terms corresponding to phenomenologically different loading sites and affinities of those sites to the drugs)[23,28] to gain more insight into their loading and release patterns and mechanisms. Loading profiles fitted by the Langmuir model stipulate that the loading is through a monolayer coverage, while those which best fit the Freundlich model suggest a multilayer coverage.[29] We found from our study that generally, the Langmuir model best describes the drug-loading process onto PUA aerogels, while the Freundlich model best describes the drug-loading process onto PIR-PUR aerogels. Also, drug release from PUA and PIR-PUR aerogels takes place in a stepwise fashion, resulting from their hierarchical porous structure. Furthermore, the Korsmeyer−Peppas and Higuchi models best fitted all the release data obtained, giving us insights into the release mechanism which was found to be predominantly through Fickian diffusion. Last, our results showed that morphology has a significant contribution to drug-loading and release profiles in aerogels, which is discussed in detail in the next section.

2. RESULTS AND DISCUSSION

2.1. Physical Characterization of PUA and PIR-PUR Aerogels. PUA and PIR-PUR aerogels were synthesized following literature procedures (Schemes S1 and S2).[13,14] The formulations of PUA and PIR-PUR aerogels of this study are given in Tables S1 and S2. These aerogels were characterized with scanning electron microscopy (SEM) to obtain topographical images of their morphologies, as shown in Figure 2A.

Since morphologies were as expected, material properties such as porosity, shrinkage, pore volume, and surface area of each PUA and PIR-PUR morphology are determined and summarized in Table S3a,b, respectively. An immediate observation from the data is that for equally porous samples of different morphologies, PIR-PUR aerogels tend to experience higher shrinkage (~5×) compared to their PUA counterparts. Also, although polyurea aerogels had a significant mesopore volume, the $V_{1.7-300\ nm}$ values of PIR-PUR aerogels were almost zero, indicating that the pore volume of PIR-PUR aerogels was mostly composed of macropores. Finally, PIR-PUR aerogels had a smaller surface area (~100×), larger particle diameter (~10×), and larger pore diameters (~50×) compared to those of PUA aerogels. To determine if any of these characteristics significantly impacted the aerogels' drug loading and release, equilibrium drug-loading capacities (Q_e) of samples from each morphology group were determined using eq 2

$$Q_e = \left(\frac{(C_o - C_e) \times \text{volume of solvent}}{\text{mass aerogel}} \right) \quad (2)$$

where C_o and C_e are the initial and equilibrium concentrations of the drug, respectively.

Previous studies have shown that porosity and surface area of aerogels play a significant role in their drug-loading and release profiles.[30] Since the surface area of aerogels is linked intimately with their morphology (e.g., the surface areas of aerogel samples with *K*-indexes 1.2−1.6 are larger than those with *K*-indexes 1.7−1.9 and are almost negligible in samples with *K*-indexes 2.0−2.2), while the porosity can be controlled through the aerogel bulk density, we selected ten samples with approximately the same porosities from different PUA and PIR-PUR morphology groups (Table 1) in this work. This ensured that any differences observed in drug loading or release from the aerogels resulted from the effect of the morphology alone.

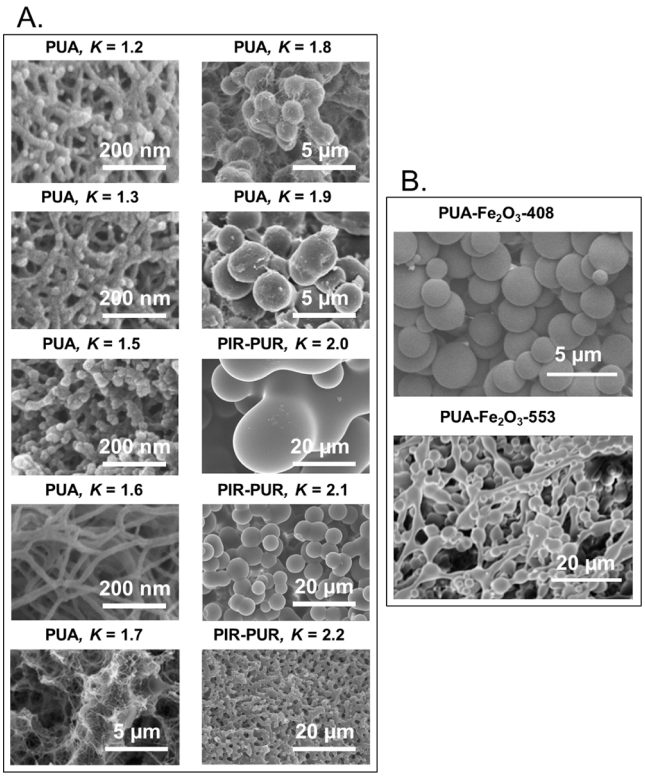

Figure 2. Morphologies identified from different PUA and PIR-PUR aerogel formulations (A) and PUA-Fe_2O_3 composite aerogels (B) (PUA-Fe_2O_3-*xx*, *xx* represents the concentration of isocyanate in mM).

2.2. Chemical Characterization of Unloaded and Drug-Loaded Aerogels. To utilize the porosity of the aerogels in loading drugs and minimize drug loading on the artificial surfaces created by pulverization, monoliths of the aerogels were used for loading drugs instead of powders. A loading method summarized in Scheme S3 was used, where saturated ethanol−water (50/50) solutions of the drugs were loaded onto the pores of the aerogels through capillary forces. The solvent was eventually removed at ambient temperature under vacuum to obtain drug-loaded aerogels. The drug-loaded aerogel (*K* = 1.2), which performed better than other morphologies in loading drugs, was characterized using FT-IR, XPS, and DSC to determine the state of the drug inside the pores of the aerogel, and results are presented in Figures S1 and 3. Figure S1 shows the FT-IR spectra of pristine polyurea aerogel and peak changes observed after loading with model drugs. Though FT-IR could show a distinction between drug-loaded and unloaded polyurea aerogels and some peaks from the drugs could be seen in their drug-loaded counterparts, the peaks were small, especially in the case of PUA-5-FU, probably because IR is a bulk technique, while the drugs in the particular samples are mostly confined to the internal surfaces. We therefore resorted to XPS, a more sensitive surface technique,

https://doi.org/10.1021/acsapm.4c01765
ACS Appl. Polym. Mater. 2024, 6, 10655−10668

Table 1. Material Properties of Selected Aerogels with Approximately Same Porosities

sample	contact angle, θ (deg.)	porosity, Π [% v/v][a]	V_{Total}[b]	$V_{1.7-300\ nm}$[c]	$V_{>300\ nm}$[d]	$\frac{V_{>300\ nm}}{V_{1.7-300\ nm}}$	BET surface area [$m^2\ g^{-1}$][e]	average pore diameter [nm][f]	particle radius [nm]
PUA, K = 1.2	90.0	78.43	2.970	1.213	1.757	1.448	232.41	108 (46)	23
PUA, K = 1.3	103.1	81.78	3.790	1.410	2.380	1.688	223.66	143 (53)	24
PUA, K = 1.5	110.6	75.65	2.540	0.457	2.083	4.558	184.23	98 (18)	24
PUA, K = 1.6	134.6	82.54	3.890	1.328	2.562	1.929	113.00	138 (47)	23
PUA, K = 1.7	140.3	80.92	3.460	0.078	3.382	43.359	24.20	577 (14)	102
PUA, K = 1.8	139.3	77.71	2.930	0.043	2.887	67.140	9.76	1172 (17)	253
PUA, K = 1.9	145.1	78.03	3.010	0.029	2.981	102.793	8.12	1505 (16)	319
PIR-PUR, K = 2.0	148.2	74.92	2.430	0.002	2.428	1214.000	1.54	6295 (6)	2280[g]
PIR-PUR, K = 2.1	153.0	73.54	2.260	0.002	2.258	1129.000	1.34	6761 (7)	830[g]
PIR-PUR, K = 2.2	151.2	68.42	1.770	0.005	1.765	353.000	3.48	2033 (7)	581[g]

[a]Via $\Pi = 100 \times (\rho_s - \rho_b)/\rho_s$. [b]$V_{Total} = (1/\rho_b) - (1/\rho_s)$. [c]$V_{1.7-300\ nm}$ from the total N_2 desorption volume. [d]$V_{>300\ nm} = V_{Total} - V_{1.7-300\ nm}$. [e]Via the t-plot method. [f]By the 4 V/σ method; for the first number, V was taken equal to $V_{Total} = (1/\rho_b) - (1/\rho_s)$; for the number in (parentheses), V was set equal to the maximum volume of N_2 adsorbed along the isotherm as P/P_o approaches 1.0. [g]From SEM using ImageJ. Average of five particles.

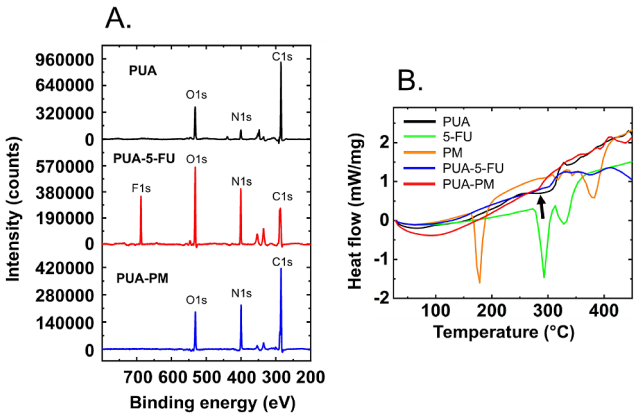

Figure 3. XPS (A) and DSC (B) of 5-FU, paracetamol (PM), PUA-5-FU, and PUA-PM samples. Drug-loaded PUA aerogels with K = 1.2, which gave the maximum drug-loading amount, were used for all analyses.

to confirm the presence of the two drugs and their association with the aerogel surfaces. Figure 3A shows the XPS spectra of native and 5-FU- or paracetamol-loaded PUA aerogels (K = 1.2). Since both drugs introduce more O and N atoms into the polyurea aerogel surfaces than what is already present in the native aerogels, the percentages of the O 1s, and N 1s peaks (Table S4) in the 5-FU-loaded PUA aerogels (18.2 and 20.1, respectively) and in paracetamol-loaded PUA aerogels (18.8 and 11.0, respectively) were higher than in native PUA aerogels (12.3 and 6.4, respectively). Also, the spectra of 5-FU-loaded PUA aerogels included a strong F 1s peak, which, of course, was absent from the paracetamol-loaded PUA aerogels.

Differential scanning calorimetry (DSC) was used to determine the physical state of drugs in the aerogel matrices. The DSC curve of PUA shows a melting temperature at 269 °C, corresponding to the small peak (indicated by the arrow) in the DSC thermogram (Figure 3B).[31] The recorded DSC curve of 5-FU, which also matches literature,[32] showed a sharp endothermic peak at ~290 °C, which was attributed to melting of crystalline 5-FU. This characteristic peak is missing from 5-FU-loaded aerogels (Figure 3B). This indicates that aerogel-loaded 5-FU is amorphous and uniformly dispersed at the molecular level in the aerogel matrix.[32] Aerogel-loaded 5-FU is amorphous, because of its close association and interaction with the aerogel matrix. Once 5-FU gets saturated in the internal surfaces of the aerogels, the excess drug precipitates as a crystalline solid due to a lack of more loading sites available to inhibit crystallization. This behavior is seen in other drug-loaded aerogels from literature studies.[33] Also, a small peak at 133 °C and a broad peak at 378 °C in the DSC curve of 5-FU-loaded aerogels were attributed to endothermic transitions resulting from the decomposition of the 5-FU-loaded PUA matrix from solid to the gaseous phase.[34] Turning to paracetamol, the DSC curve showed a sharp peak at ~170 °C consistent with literature.[35] This characteristic peak of crystalline paracetamol was missing from the DSC curve of paracetamol-loaded aerogel, indicating that paracetamol-loaded in the aerogel was amorphous with the same implications about its topological relationship with the skeletal network as in the case of 5-FU.

2.3. Microstructural Characterization of Drug-Loaded Aerogels. According to scanning electron microscopy (SEM), all aerogels used in this work kept their morphologies after drug loading. This is demonstrated in Figure 4 with the

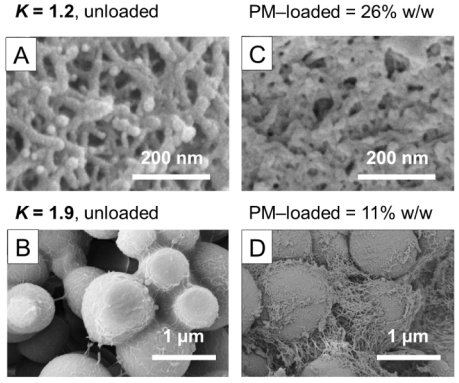

Figure 4. Morphology of drug-unloaded K = 1.2 (A) and K = 1.9 (B) aerogels and their paracetamol-loaded counterparts (C,D), respectively.

maximum (26% w/w, K = 1.2) and minimum (11% w/w, K = 1.9) paracetamol-loaded samples in comparison with the drug-unloaded samples. SEM images of other samples are shown in Figure S2.

2.4. Quantification of Drug Loading onto PUA and PIR-PUR Aerogels. To correlate drug loading with morphology, we determined the equilibrium drug-loading capacities of samples with different morphologies but approximately the same porosities. Figure 5A,B shows that the loading capacities

https://doi.org/10.1021/acsapm.4c01765
ACS Appl. Polym. Mater. 2024, 6, 10655−10668

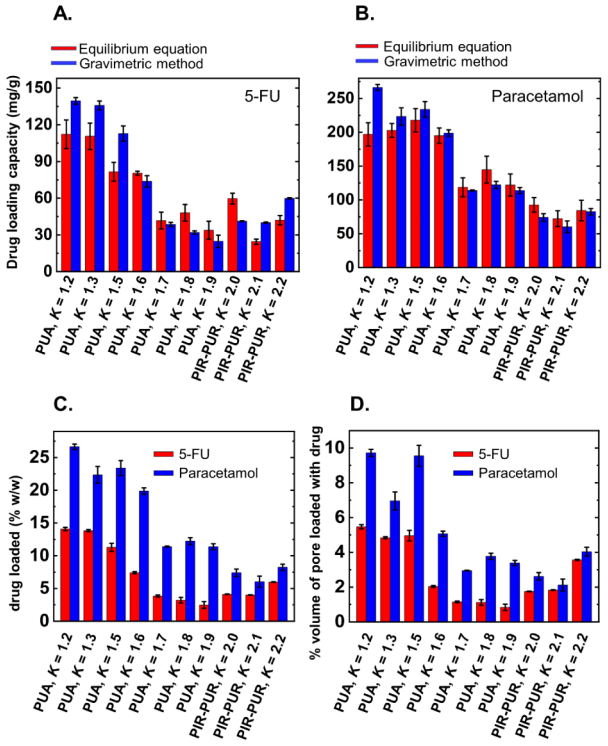

Figure 5. Drug-loading capacities in mg/g of 5-FU (A) and paracetamol (B), percent drug-loading capacities (C), and volume of pores filled with drugs (D) of aerogels with approximately same porosities.

of aerogels determined using either eq 2 or by the gravimetric analysis method (eq 3) gave approximately the same results:

$$\%\frac{\text{w}}{\text{w}} = \left(\frac{\text{mass of drug} - \text{loaded}}{\text{mass of aerogel}}\right) \times 100 \quad (3)$$

In both 5-FU and paracetamol-loaded samples, the loading amounts decreased from K = 1.2 to K = 2.2 in a similar pattern.

Morphologies with higher surface areas (K = 1.2−1.6) could have uptake of larger amounts of drugs compared to those with lower surface areas (K = 1.7−2.2) though all samples had about the same porosities. Also, since both the completely bald PIR-PUR aerogels (K = 2.0−2.2) and the almost-bald PUA aerogels (K = 1.8−1.9) have only a small difference in their surface area, their drug-loading amounts were almost the same. The slight differences in the surface area and drug-loading amounts of the two systems can be attributed to their surface chemistry (urea vs urethane groups). This suggests that other aerogel systems with approximately the same porosity, morphology, and surface chemistry as those of PUA and PIR-PUR aerogels can have similar drug-loading capacities.

It is observed from Figure 5 that samples with caterpillar-like morphology (K = 1.2) had taken up the largest amount of drug compared to all the remaining morphologies. This is because K = 1.2 has a higher surface area compared to that of K = 1.7−2.2. Although the material properties (Table 1) of K = 1.2 and K = 1.3 are approximately the same, K = 1.2 is unique since its surface is hydrophilic (contact angle = 90 °C), while all other morphologies are hydrophobic (contact angle >100 °C). Last, it is observed from Figure 5 that the amount of paracetamol loaded onto the aerogels was ∼2× greater than that of 5-FU. This can be attributed to the higher solubility of paracetamol (20 mg/mL) in ethanol−water (50/50) solution, which was used as a solvent compared to that of 5-FU (6 mg/mL), considering that the difference between the molecular weights of the two drugs is not large.

It is noticed in Figure 5D that from almost bald (PUA, K = 1.9) to completely bald microspheres (spheroidal-PIR-PUR, K = 2.1), the pores occupied with drug for PUA aerogels were greater than those for PIR-PUR aerogels. Since there is a large reduction in the macropore to mesopore volume ratio in fused nanostructured PUA (4.558) compared to that of PIR-PUR (1214) (Table 1) and a significant reduction in the surface area of fused spheres of PIR-PUR (∼200× lower) compared to that of PUA, it presupposes that the drugs were loaded inside "inner" mesopores first before occupying the surfaces of "outer" macropores.

The fact that aerogels with smaller diameters and larger surface areas (K-indexes 1.2−1.6) have uptake of more drugs compared to those with larger pore diameters and smaller surface area (K indexes 1.7−2.2) (Figure 5) further confirms that the drug-loading process is associated with uptake of drugs onto the surfaces of macropores, mesopores, or fibers depending on the morphology being studied.

Figure 5D shows that the % v/v utilization for fused nanostructured PUA was greater than that of PIR-PUR although all the samples analyzed had approximately the same porosities and the same loading conditions were employed to load drugs onto their porous network. Also, the percent porosity utilization (Π_u) for drug storage in K = 1.2−1.5 reached ∼10% v/v and that of K = 2.2 reached ∼5% v/v, which is greater than the percent porosity utilization values of all the remaining morphologies (∼2% v/v). This can be attributed to the larger surface area associated with morphologies of PUA aerogels at K−indexes of 1.2−1.5. PIR-PUR aerogels at K = 2.2 recorded the largest drug-loading amount after filling ∼5% of their pores. This observation seen with PIR-PUR morphologies may be due to the equally sized particle and pore diameters in bicontinuous nanostructures, which increase their surface areas and readily available loading sites.

Since the drugs load onto the surface of the aerogel pores, the amount of drug needed to cover the BET surface area (theoretical drug uptake), assuming monolayer coverage, was calculated by gaining insights from a previously reported procedure.[36] For each morphology, the theoretical drug uptake in moles was calculated by dividing the BET surface area by the area occupied by one molecule of the drug (5-FU = 31.139 Å^2, paracetamol = 40.170 Å^2) and Avogadro's number (6.02×10^{23} mol^{-1}). The area occupied by one molecule of the drug was obtained through molecular modeling using a Chem3D software package.

For each morphology, the drug-loading values obtained using gravimetric analysis were compared with the theoretical drug uptake, and results are presented in Figure 6 and Table S5a.

It is seen from Figure 6 that the entire surface of the carriers is covered with drugs (the amount of drug needed to cover the surface of the aerogels is the same or lower than the amount of drug loaded). The differences in the amount of drug needed to cover the surface of the aerogels and the actual amount of drug that was loaded onto the surface show that more drugs load onto the surfaces of already loaded drugs to form a bilayer or a multilayer drug-loading phenomenon. The multilayer drug-loading phenomenon seen in these drug carriers inspired the

https://doi.org/10.1021/acsapm.4c01765
ACS Appl. Polym. Mater. 2024, 6, 10655−10668

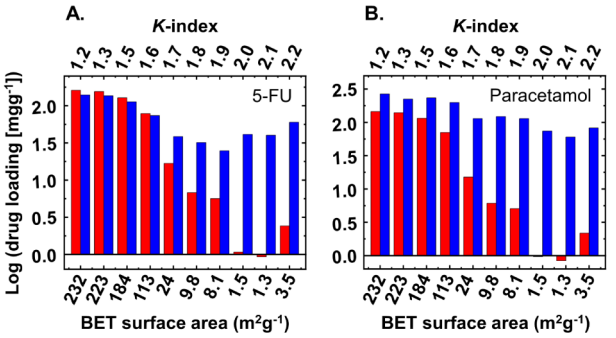

Figure 6. Amount of drug 5-FU (A) and paracetamol (B) needed to cover the surface area (mgg^{-1}) (red) and the actual amount of drug loaded (mgg^{-1}) (blue) onto the aerogels.

determination of the volume of pores occupied with drugs for each morphology (Figure 5D).

Figure 6 shows that the amount of drug needed to cover the surface of fused nanostructured PUA (K = 1.5) was greater than that of PIR-PUR (K = 2.0). Also, comparing almost bald (PUA, K = 1.9) to completely bald microspheres (PIR-PUR, K = 2.1), the pore surfaces covered with drugs for PUA aerogels were greater than those for PIR-PUR aerogels. This can be attributed to the significant reduction in the macropore to mesopore ratio in fused nanostructured PUA (4.558) compared to that of PIR-PUR (1214) and bald microspheres (102) compared to spheroidal (1129) (Table 1). It is obvious from Table 1 that although the macroporous spaces in PUA and PIR-PUR are within a narrow range, PUA aerogels (especially, K = 1.2−1.6) have a significantly larger mesopore volume compared to PIR-PUR aerogels, which also contributes to the difference in the surface area between PUA and PIR-PUR aerogels (~200×). Since PUA aerogels loaded more than twice the amount of drug loaded onto PIR-PUR aerogels and their porosities are within a narrow range, it presupposes that drugs were loaded in a multilayer fashion onto the "inner" mesopores first before covering the surfaces of the "outer" macropores.

Since the surface area, which is seen here to contribute significantly to drug loading, is affected by the morphology of the aerogels as seen from Table 1 and reported in other studies,[37] it was reasonable to conclude that morphology had a significant effect on the loading of drugs onto the aerogels. Based on these findings, we probed further to see if the morphology can be used as a tool to predict the drug-loading capacity of aerogels. This was done by comparing our drug-loading results for PUA aerogels to those reported for other aerogels with similar morphologies. Drug-loading data for some novel PUA-Fe_2O_3 composite aerogels were also compared to PIR-PUR aerogels with equivalent morphologies (Figure 2B). Our findings, summarized in Table 2, indicated that different aerogel systems with the same morphologies as those of PUA and PIR-PUR aerogels loaded approximately the same amount of drugs as their PUA and PIR-PUR aerogel counterparts.

2.5. Estimation of the Maximum Drug-Loading Capacity of Aerogels. To further probe the effect of morphology on drug loading onto aerogels, the Langmuir and Freundlich models were used to estimate the maximum amount of drug that can be loaded onto each morphology under the same conditions. The nonlinear forms of the Langmuir and Freundlich equations are given in eqs 4 and 5, respectively. The Langmuir fit was used to determine the maximum drug-loading capacity for each morphology, while the Freundlich fit was used to determine the loading mechanism and feasibility:

$$Q_e = \frac{Q_m b C_e}{1 + b C_e} \tag{4}$$

$$Q_e = K_f C_e^{1/n} \tag{5}$$

where Q_e (mg/g) is the equilibrium loading capacity, C_e (mg/mL) is the equilibrium concentration of 5-FU, Q_m (mg/g) is the maximum drug-loading capacity, b (mL/mg) is the Langmuir binding constant, K_f (mg/g) is the approximate indicator of loading capacity, and n is the Freundlich heterogeneity factor.

The Langmuir model is preferred to the Freundlich model in estimating the maximum drug-loading capacity since the latter does not predict the adsorption capacity of drug saturation on the adsorbent surface.[27] In this study, since the drug is loaded onto the aerogels on a molecular level (amorphous form) as determined from DSC characterization,[42] both Langmuir and

Table 2. Comparison of Drug-Loading Amounts of Different Aerogels with Those of PUA and PIR-PUR Aerogels with Similar Morphologies

aerogel	morphology	porosity	surface area (m^2g^{-1})	drug	drug loading (% ww^{-1})	references
PUA (K = 1.2 or 1.3)	caterpillar-like, worm-like, or rod-like	78.4	110.0	PM	27	-
Balangu (*Lallemantia royleana*) seed mucilage aerogel		-	95.74		33 ± 2	38
PUA (K = 1.5)	fused nanostructures	75.7	104.0	PM	23.0	-
polyethylenimine-grafted cellulose nanofibrils aerogel		-	79.0	sodium salicylate (NaSA), similar molecular weight as PM	28.0	39
PUA (K = 1.6)	entangled nanofibers	82.5	113.0	PM	20.0	-
cellulose triacetate aerogel		~95.0	162.0		19.8	40
PUA (K = 1.9)	microspheres	78.0	8.1	5-FU	3.0	-
graphene oxide/hydroxypropyl cellulose/chitosan hybrid aerogel		-	-		3.6	41
PIR-PUR (K = 2.1)	spheroidal	73.5	1.3	5-FU	4.0	-
PUA-Fe_2O_3-408		72.0	-		6.1	-
PIR-PUR (K = 2.2)	bicontinuous	68.4	3.5	5-FU	6.0	-
PUA-Fe_2O_3-553		82.9	-		6.0	-

https://doi.org/10.1021/acsapm.4c01765
ACS Appl. Polym. Mater. 2024, 6, 10655−10668

Table 3. Summary of Nonlinear Langmuir and Freundlich Fit Parameters for 5-FU and Paracetamol Loading

	Langmuir isotherm parameters			Freundlich isotherm parameters		
5-FU-loaded aerogels	Q_m (mg g^{-1})	b (L mg^{-1}) × 10^{-6}	R^2	K_f (mg g^{-1}) × 10^{-5}	$1/n$	R^2
PUA, K = 1.2	656.842	20.000	0.984	139.000	1.296	0.991
PUA, K = 1.3	1863.237	10.000	0.973	208.000	1.270	0.976
PUA, K = 1.5	1149.083	60.000	0.984	12156.000	0.916	0.982
PUA, K = 1.6	4181.379	10.000	0.986	83.000	1.457	0.917
PUA, K = 1.7	1682.743	16.400	0.960	1250.000	1.112	0.854
PUA, K = 1.8	1339.595	30.000	0.943	25.800	1.629	0.960
PUA, K = 1.9	144.158	113.000	0.974	38.690	1.112	0.945
PIR-PUR, K = 2.0	1146.825	11.000	0.947	120.500	1.290	0.953
PIR-PUR, K = 2.1	1090.876	22.000	0.893	6.520	1.750	0.926
PIR-PUR, K = 2.2	808.614	23.000	0.947	15.000	1.604	0.961
Paracetamol-Loaded Aerogels						
PUA, K = 1.2	1519.623	17.500	0.998	24561.502	0.750	0.990
PUA, K = 1.3	3649.889	6.240	0.988	4552.036	0.918	0.935
PUA, K = 1.5	3184.484	7.250	0.877	143461.380	0.556	0.833
PUA, K = 1.6	4181.383	0.902	0.967	29662.653	0.561	0.982
PUA, K = 1.7	2774.890	5.580	0.921	2.751	1.649	0.978
PUA, K = 1.8	1653.510	4.470	0.905	53679.540	0.740	0.740
PUA, K = 1.9	493.515	64.100	0.981	37186.467	0.677	0.975
PIR-PUR, K = 2.0	812.404	143.337	0.982	141866.165	0.628	0.959
PIR-PUR, K = 2.1	1799.023	31.400	0.974	15129.937	0.862	0.978
PIR-PUR, K = 2.2	462.608	11.500	0.830	370.379	1.014	0.927

Freundlich models were used in evaluating the maximum drug-loading capacity. Table 3 presents nonlinear Langmuir and Freundlich fit parameters for all morphologies, and their fits are shown in Figures S4 and S5. The parameters of isotherms (Q_m, b, K_f, and n) were calculated using eqs 4 and 5 and were used to characterize the loading process. The linearized forms of the models were not included since, though they are easy and straightforward, making the isotherms linear creates propagating errors, which can cause erroneous predictions of the parameters. The use of nonlinear regressions for the Langmuir and Freundlich models is therefore recommended in calculating the model parameters.[43]

The results indicate that morphologies with larger surface areas (K = 1.2−1.6) experienced greater maximum drug-loading capacities, with nanofibrous morphology (K = 1.6) recording the greatest value among all the morphologies. This is because in porous drug carriers with small mesoporous space, the surface area correlates directly with their maximum drug-loading capacity.[44]

After determining the maximum drug-loading capacities in PIR-PUR aerogels (Table 3), we found that bicontinuous nanostructures (K = 2.2) had uptake of a lesser quantity of drugs compared to spheroidal (K = 2.1) and fused spheres (K = 2.0). This observation can be attributed to the large particle radii in K = 2.0−2.1, which causes them to have a larger macroporous surface (∼2×) and larger pore volume (∼3×) for drug loading than those of bicontinuous morphology.[14]

Three observations are apparent from the fits. First, Figures S4 and S5 show that the amount of drug which is loaded onto the aerogels increases when the initial drug concentration is increased. Also, as seen in Tables 1 and 3, morphologies with smaller pore diameters (<200 nm) (K = 1.2−1.6) mostly fit the Langmuir model, while those with larger pore diameters (>500 nm) (K = 1.7−2.2) mostly fit the Freundlich model. It is also seen from Table 1 that aerogels with K = 1.2−1.6 are highly mesoporous compared to those with K = 1.7−2.2. This suggests that higher surface area morphologies with K-indexes 1.2−1.6 undergo near monolayer drug-loading processes covering the surfaces of mesopores and macropores, while those with K = 1.7−2.2 undergo multilayer drug-loading processes onto macroporous surfaces.[45] Results from the models confirm our previous observation (Figure 6), as the amount of drug loaded onto morphologies with K-indexes 1.2−1.6 was approximately the same as the amount of drug needed to cover the surface area (monolayer loading), especially with 5-FU loading (this agrees with the Langmuir model). On the other hand, for both 5-FU and paracetamol, the amount of drug loaded onto morphologies with the K-index in the range of 1.7−2.2 exceeded the amount of drug needed to just cover the surface signifying a multilayer loading process, which is more suited to the Freundlich model. Last, the loading data for 5-FU fit better to the Freundlich model compared to the Langmuir model, while the opposite is observed with the loading data for paracetamol. This can be attributed to the larger number of 5-FU molecules, which can occupy the same surface area as a smaller number of paracetamol molecules. The large 5-FU molecules available for loading onto a smaller surface area can cause multilayer adsorption of 5-FU which is associated with the Freundlich model. Since Langmuir and Freundlich isotherms describe a monolayer and multilayer drug-loading process, respectively, it presupposes that paracetamol has a stronger affinity to the surface of the aerogels compared to 5-FU. This is reasonable since paracetamol has more functional groups (−OH and −NH), which can form hydrogen bonds with PUA and PIR-PUR aerogels compared to 5-FU (only −NH).

Observations made on drug loading onto PUA aerogels (Figure 6) and the maximum drug loading data from Table 3 follow a unique pattern from K = 1.2−1.5 and from K = 1.6−1.9. This pattern is like the results obtained by Taghvaee et al. for several other properties of PUA aerogels analyzed.[13]

The Langmuir and Freundlich constants were determined by regression of the fitting curve. The Freundlich isotherm parameter ($1/n$) in eq 5 represents the degree of heterogeneity

https://doi.org/10.1021/acsapm.4c01765
ACS Appl. Polym. Mater. 2024, 6, 10655−10668

(nonidentical loading sites) on the surface of the adsorbent. Loading of drugs onto a nonidentical loading site requires different energies and therefore influences the feasibility of the loading process. Less heterogeneity in drug loading (i.e., the drug-loading process having an almost equal loading affinity to all loading sites) corresponds to an easier drug-loading process since there is a more uniform surface energy distribution on all loading sites, has less energy toward the adsorbate, and hence requires less energy for drug loading. An easier drug-loading process that has a low enthalpy of adsorption mostly fits the monolayer Langmuir equation. Generally, $1/n$ values which are less than 1 and higher values of n are more desirable for the drug-loading process.[46] The K_f value indicates an approximate drug-loading capacity. Larger K_f values correspond to greater drug-loading capacities of aerogels and vice versa.[47] Results from the nonlinear Langmuir and Freundlich fits for 5-FU (Table 3) indicate that all the morphologies have a high heterogeneity ($1/n \geq 1$) in 5-FU loading, which makes loading of 5-FU onto their porous network difficult. On the other hand, the heterogeneity parameter ($1/n$) for paracetamol-loaded aerogels is less than one, and hence, they experience an easier drug-loading process. This possibly explains the lower 5-FU loading capacities compared to paracetamol aside from the fact that the former has a lower solubility in an ethanol/water (50/50) solution.

The data obtained also presupposes that loading of paracetamol onto aerogels is highly associated with a chemisorption process (stronger affinity for the adsorbent's surface) since ($1/n$) is between 0 and 1, and that of 5-FU loading onto aerogels occurs through a physisorption process (weaker affinity to the adsorbent's surface).[42] Paracetamol loading can be associated with a chemisorption process since, though hydrogen bonds are mostly classified under physisorption, they can be interpreted as a chemisorption process if bonds are very strong.[48]

2.6. Drug Release from PUA and PIR-PUR Aerogels. Though the capacity of an aerogel to store drugs is a necessary condition for a drug delivery system, drug loading alone is not sufficient, since loaded drugs must also be released to the target site. We therefore studied how morphology influences the drug release patterns from these aerogels. Since the morphologies of aerogels were maintained after drug loading (Figure 4), it was reasonable to use the same drug-loaded samples to study their release profiles; however, samples with higher drug loadings were reloaded with less concentrated drug solutions so that the drug loadings and mass for each drug-loaded aerogel used for the release study remained practically the same.

Drug release rates and mechanisms from each morphology group were studied spectrophotometrically using two methods: (a) releasing the loaded drug into PBS buffer solution (pH = 7.4) continuously for 0.5 or 24 h or (b) releasing the drug for 72 h (monitored at 0.5, 1, 3, 6, 12, 24, 48, and 72 h). For the latter, aliquots taken for spectroscopic measurements were replenished with an equal volume of a fresh PBS buffer solution. Typical data for the first method are presented in Figure 7, while the second method is discussed in the next section.

We notice in Figure 7 that PUA aerogels (K = 1.2−1.3) and PIR-PUR aerogels (K = 2.0) experienced the slowest release. This can be attributed to the curved and cage-like pore geometry of these morphologies since nanostructures with those geometries have been reported to give a slower release of

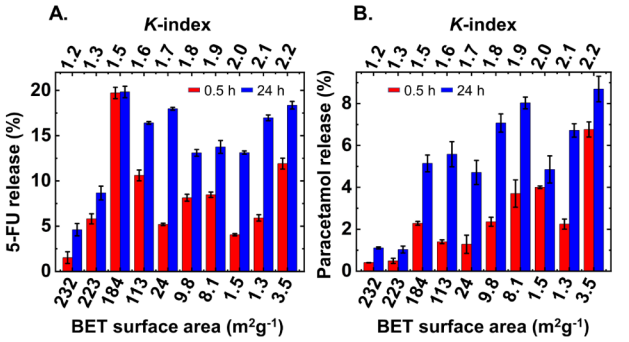

Figure 7. Percent of drug released from aerogels in 0.5 h (red) and 24 h (blue) for 5-FU (A) and paracetamol (B).

drugs. This results from the long nonlinear diffusion pathways created by these cage-like structures for the release of drugs.[49] For both drugs, aerogels with morphologies at K = 1.5 and 2.2 experienced the fastest release rates compared to the remaining morphologies. This is attributed to the lack of crevices on the skeletal frameworks making drugs easily available for dissolution and release compared to the other morphologies whose nanostructures are not fused.[50] In PIR-PUR aerogels, although fused spheres are expected to have a faster drug release, they show a slower release compared to that of bicontinuous morphology. This is expected since bicontinuous structures resemble the fused nanostructured PUA aerogel. Both aerogels have smaller interconnected pore openings compared to their corresponding morphologies (pore diameter in bicontinuous PIR-PUR (2033 nm) is smaller than that in other PIR-PUR morphologies, and the pore diameter in fused nanostructured PUA (98 nm) is smaller than that in the remaining PUA aerogel morphologies). Also, with bicontinuous structures, the pores and particles are approximately the same size. These morphological features create a short linear diffusion pathway for the release of drugs in contrast to the long drug release pathway in fused spheres caused by their large nonuniform cage-like porous structures and therefore give a faster drug release for bicontinuous nanostructures.[51]

Aside from the smaller and uniform pore diameters in bicontinuous morphology giving a faster release compared to fused spheres, the faster release in bicontinuous morphology can also be attributed to their smaller particle size (radius = 581 nm) compared to fused spheres (radius = 2280 nm). It is reported that nanostructures with smaller particle sizes give a faster release than those with larger particle sizes since smaller nanostructures tend to generate a large surface area for drug dissolution and release. This is seen from Table 1 where the surface area in bicontinuous morphology (3.48 m^2g^{-1}) is greater than that in fused spheres (1.54 m^2g^{-1}).[52]

Except for PUA morphologies with hair-like structures, PUA aerogels mostly released drugs slower than PIR-PUR aerogels. This is because PUA aerogels are more highly mesoporous than PIR-PUR aerogels. Mesopores play a significant role in releasing drugs slowly as it creates a hierarchical porous nanostructure of randomly porous aerogels.[53] The hierarchically porous nanostructure which is dominant in PUA creates a significantly heterogeneous adsorbent−adsorbate interface with a lower surface energy than that in PIR-PUR. This low surface energy demands a higher energy for drug release, which accounts for a lower release seen in PUA with particulate morphology compared to PIR-PUR morphologies.

https://doi.org/10.1021/acsapm.4c01765
ACS Appl. Polym. Mater. 2024, 6, 10655−10668

On the other hand, the hair-like nanostructures in PUA aerogels (K = 1.6−1.9) present a different surface with a higher surface energy than particles, and therefore, less energy is required for drug release.[54] As a result, nanofibrous morphology (K = 1.6) experiences a higher drug release like those in PIR-PUR. Morphologies with particulate and hair-like structures (K = 1.7−1.9) present two different surfaces for drug release and hence receive an intermediate drug release rate (neither fast nor slow). Also, as the release medium penetrates the porous network, drugs on the surface of "deeper" pores (mesopores) are covered by the ones on the outer surfaces defined by the macroporous space and are therefore released later. More slow release results from the strength of H-bonds, formed between drugs and with PUA itself, within the confined mesoporous space. Figure 7 also indicates that as a greater percentage of loaded drug is released, cocoon-like nanostructures (K = 1.7) tend to experience a faster release compared to that in microspheres with hair-like (K = 1.8) and bald microspheres (K = 1.9). Similarly, the amount of fibers on K = 1.7 is greater than that in K = 1.8 and 1.9. This supports the initial suggestion that nanofibers contribute to the fast release of drugs from PUA morphologies. Drug release from PUA aerogels takes place in a stepwise fashion (Figures 8, S6 and S7). This suggests that the drug is

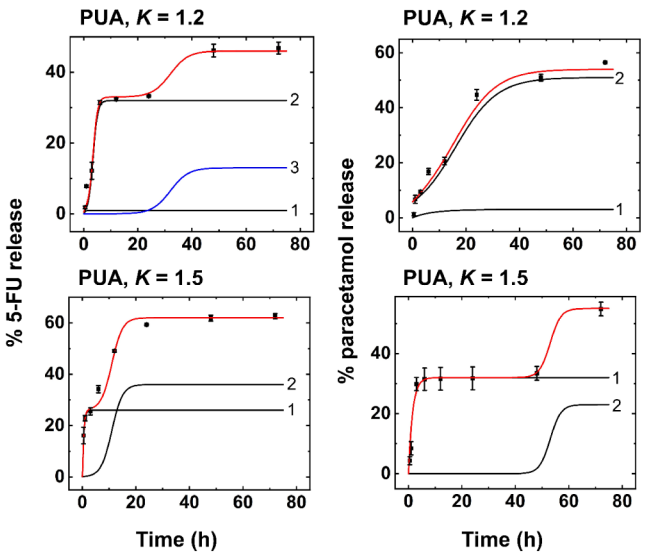

Figure 8. Drug release in phosphate buffer (pH = 7.4) from various drug-loaded PUA (K = 1.2 and 1.5) aerogels (5-FU-loaded is ∼136 mgg^{-1}, and paracetamol-loaded is ∼557 mgg^{-1}).

released in stages from both the mesoporous and macroporous surfaces. The stepwise release phenomenon is also seen in the release profiles in PIR-PUR aerogels though their pore volumes are constituted mainly by macropores and have lesser hierarchical porous structures compared to PUA. Since drugs are released predominantly from their macropores, these release patterns observed can be attributed to their extremely large particle sizes which are known to give a sigmoidal drug release pattern.[55]

2.7. Mathematical Modeling of Drug Release from Aerogels. To enable us to kinetically model the effect of morphology on drug release, release of both drugs from each morphology group was monitored at regular time intervals (0.5, 1, 3, 6, 12, 24, 48, and 72 h) in PBS buffer (pH = 7.4), and the obtained data were fitted to select mathematical models as described in the next sections.

2.7.1. Fitting Release Data with a Sigmoidal Drug Release Equation. Drug release data for all morphologies were fitted with eq 6, which consists of an exponential component (curve 1) and two sigmoidal components (curves 2 and 3):[23]

$$\%\ \text{drug release} = \underset{(\text{curve1})}{A_1[1 - \exp[C_1(B_1 - t)]]} + \underset{(\text{curve2})}{\frac{A_2}{[1 + \exp[C_2(B_2 - t)]]}} + \underset{(\text{curve3})}{\frac{A_3}{[1 + \exp[C_3(B_3 - t)]]}} \quad (6)$$

The individual curves 1−3 are included in the release profile for each morphology as indicated in Figures 8 and S6 and S7, while their corresponding coefficients A_i, B_i, and C_i ($1 \le i \le 3$) are given in Table S6.

Eq 6 was inspired by another type of mass-transfer-controlled surface processes happening at different energy levels[23] similar to the faradaic processes of several redox-active substances happening at the same electrode.[55] Here, different amounts of drug (A_i) are released from the aerogels into PBS buffer (the release medium) by concentrating the drugs close to the solid surface (within <1 mm) through agitation. B_i describes the drug release, and C_i describes the kinetics of the process. Therefore, curve 1 addresses the smooth release of drugs loaded onto the aerogels, while curves 2 and 3 describe situations where the drug released equilibrates with other forms of itself.

Gaining insights from the explanation above, A_i quantifies the contribution from each component, B_i quantifies the position of each curve at each time point (t), and C_i quantifies the release profiles, that is, how fast or slow the release is. Therefore, the sum of coefficients A_i represents the total amount of drug released within the period of the drug release studies and $B_1 < B_2 < B_3$ as expected. Release is faster for $C_1 > 1$ and slower for $C_1 < 1$.

Two observations are immediately apparent in Figures 8 and S6 and S7: release of both drugs from K = 1.2 and 1.9 was more protracted than the remaining morphologies, and the release of both drugs from morphologies with K-indexes 1.5 and 1.9 could be fitted with only two terms (curve 1 and curve 2). Comparing all the aerogel morphologies studied, B_1 = 0 and $A_1 > A_2, A_3$ for the release of both drugs from bicontinuous morphology (K = 2.2). Also, both drugs released fastest from bicontinuous and fused nanostructures (K = 1.5 and 2.2) as seen in their A_1 value being the largest among their counterparts (except for K = 1.8 which was unexpectedly high for 5-FU release). These observations indicate that the largest portion of the drugs was held loosely in bicontinuous and fused nanostructured morphologies and was released faster starting from the moment the samples were placed in the release medium.

Considering the inferences from the fits obtained, the significant mesopore−macropore ratios seen in Table 1, and knowledge of the hierarchical porous nanostructure of randomly porous aerogels,[56] it is reasonable to conclude that drugs loaded onto the surfaces of "deeper" pores (mesopores) are "protected" by drugs confined on the outer surfaces that define the macroporous space and are therefore released later.

https://doi.org/10.1021/acsapm.4c01765
ACS Appl. Polym. Mater. 2024, 6, 10655−10668

Table 4. Potential for Drugs to Be Released in a Controlled or Sustained Manner[a]

5-FU-loaded aerogels	maximum zero-order release time (tmax-0) (h)	R^2	percent released at tmax-0 (%)	maximum first-order release time (tmax-1) (h)	R^2	percent released at tmax-1%)
PUA, K = 1.2	6	0.960	31.50 ± 0.55	6	0.956	31.46 ± 0.55
PUA, K = 1.3	24	0.962	38.14 ± 1.75	24	0.965	38.14 ± 1.75
PUA, K = 1.5	24	0.920	59.30 ± 0.24	24	0.962	59.31 ± 0.24
PUA, K = 1.6	24	0.902	77.00 ± 3.89	72	0.979	94.95 ± 0.33
PUA, K = 1.7	12	0.982	45.77 ± 1.02	12	0.960	45.77 ± 1.03
PUA, K = 1.8	12	0.920	47.60 ± 0.54	48	0.900	65.98 ± 3.03
PUA, K = 1.9	6	0.985	34.80 ± 1.96	48	0.900	55.65 ± 1.67
PIR-PUR, K = 2.0	24	0.942	65.67 ± 1.10	24	0.973	65.67 ± 1.10
PIR-PUR, K = 2.1	3	0.990	49.23 ± 3.33	3	0.985	49.23 ± 3.33
PIR-PUR, K = 2.2	6	0.989	58.32 ± 3.21	24	0.927	79.04 ± 3.04
Paracetamol-Loaded Aerogels						
PUA, K = 1.2	24	0.972	44.72 ± 1.98	72	0.901	31.46 ± 0.55
PUA, K = 1.3	24	0.900	51.90 ± 1.49	24	0.948	51.90 ± 1.49
PUA, K = 1.5	a	a	a	3	0.997	25.51 ± 1.38
PUA, K = 1.6	72	0.900	69.16 ± 1.42	72	0.948	69.16 ± 1.42
PUA, K = 1.7	6	0.987	25.50 ± 1.09	72	0.900	53.09 ± 0.13
PUA, K = 1.8	72	0.942	47.09 ± 1.31	72	0.958	47.09 ± 1.31
PUA, K = 1.9	72	0.936	38.40 ± 1.31	72	0.955	38.41 ± 1.31
PIR-PUR, K = 2.0	a	a	a	72	0.914	59.99 ± 1.47
PIR-PUR, K = 2.1	3	0.900	32.56 ± 0.57	3	0.923	32.56 ± 0.57
PIR-PUR, K = 2.2	6	0.961	29.95 ± 3.58	6	0.974	29.95 ± 3.58

[a]–Data do not follow the release profile.

Also, drugs can be released quickly or slowly, depending on the location of the drugs (mesopores or macropores) and different surface energies associated with different pore surfaces within the different morphologies onto which drugs were loaded. More protracted release (lower C_i values) is attributed to the strength of the interactions within the confined mesoporous space. The interactions within the mesoporous space include hydrogen (H) bonding of drugs with themselves and with the −NH−C(═O)−NH− groups of the PUA and PIR-PUR frameworks. Hence, by keeping the release medium constant (PBS buffer, pH 7.4), paracetamol, with more functional groups capable of developing H-bonding (−OH and −NH groups), shows a more protracted release from the innermost locations in the framework than release of 5-FU (curves marked "'3'" are mostly protracted for paracetamol than for 5-FU as shown in Figures 8 and S6 and S7).

2.7.2. Fitting Drug Release Data to Zero-Order, First-Order, Higuchi, and Korsmeyer–Peppas Kinetic Models. Fitting the release data to the sigmoidal equation above gives us information on the release patterns and confirms that drugs are released from the surfaces of mesopores, macropores, and fibers. However, the sigmoidal release profiles fail to give some important information such as the potential of the model systems (PUA and PIR-PUR aerogels) to control and/or sustain drug release and the mode of drug release (whether it is through Fickian or non-Fickian diffusion or erosion/collapse of the aerogel matrix). We therefore fitted our data to other mathematical drug release models,[28] the zero-order (eq 7), first-order (eq 8), Higuchi (eq 9), and Korsmeyer–Peppas model (eq 10), to gain more insights into the mechanism of drug release from these systems.

$$Q_t = Q_o + K_o t \tag{7}$$

$$\mathrm{Log}Q_t = \mathrm{Log}Q_o + \frac{K_t}{2.303} \tag{8}$$

$$Q_t = a \times t^{1/2} \tag{9}$$

$$Q_t = k \times t^n \tag{10}$$

where Q_t is the cumulative amount of drug released in time t, Q_o is the initial amount of drug in the solution (typically, $Q_o = 0$), K_o is the zero-order release constant expressed in units of concentration/time, a is the Higuchi dissolution constant, k is the release rate constant, and n is the release index.

Due to the usefulness of controlled-release technologies which are best characterized by a release profile's ability to fit zero-order drug release kinetics in pharmaceutics,[57] release from all morphologies were analyzed for their potential to follow zero-order release kinetics as indicated in Table 4. Though the release of drugs from the nanostructures was studied within a 3-day period, the R^2 values for the period in which the release follows a controlled-release profile are given in Table 4, while the fits and R^2 values for the entire 3-day period of release studies are given in Figures 9 and S8. Table 4 also shows how best the release profile of each morphology fits first-order kinetics.

Morphologies with K-indexes 1.6–2.0 follow first-order release kinetics. Hence, they are best suited for sustained-release formulations.[58] It is observed from Table 4 that nanofibrous morphology with a K-index of 1.6 is the most suitable for controlled-release technology compared to all other morphologies, as ∼70% of both 5-FU and paracetamol stored in it undergo zero-order release within 24–72 h. Considering that the particle sizes of K = 1.7–1.9 (diameter >200 nm) and K = 2.0 (diameter = 4560 nm) are greater than those of their corresponding PUA aerogels (diameter <50 nm) and PIR-PUR aerogels (diameter <1000 nm), the results obtained are expected, since it is reported that nanostructures with larger particle sizes can be utilized to achieve sustained drug release.[50]

https://doi.org/10.1021/acsapm.4c01765
ACS Appl. Polym. Mater. 2024, 6, 10655−10668

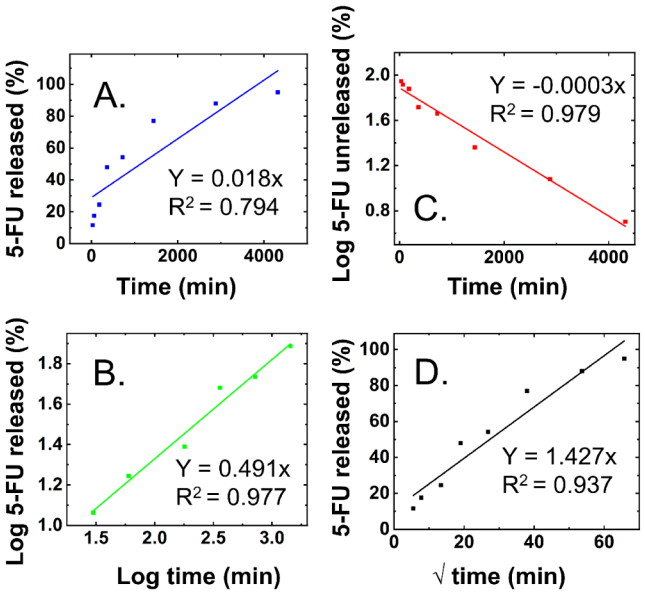

Figure 9. Fitting 5-FU release data for nanofibrous morphology (K = 1.6) using various mathematical drug release models: zero-order release (A), Korsmeyer−Peppas (B), first-order (C), and Higuchi models (D).

All release data also fitted the Korsmeyer−Peppas model (Figures S10 and S11), which describes the release mechanism of drug from nanocarriers. This observation suggests that drug release from all the aerogels was governed by diffusion.[59] The Korsmeyer−Peppas model is characterized by the value of parameter n in eq 10. If $n < 0.5$, the sustained-release mechanism is dominated by Fickian diffusion, if $0.45 < n < 0.89$, the release mechanism is mainly influenced by non-Fickian diffusion, and when $n > 0.89$, the release mechanism is mainly through a bone erosion effect of the drug-loaded aerogel.[60] From the obtained data shown in Table S7, all 5-FU release from aerogels was governed by Fickian diffusion and paracetamol release followed Fickian diffusion mechanism for all morphologies except K = 1.8 and 1.9.

Finally, drug release data for all morphologies fitted the Higuchi model (Figures S8 and S9) which presupposes that matrix swelling and dissolution of drug-loaded aerogels in the release medium were negligible, and drug diffusivity through the aerogels' porous network was constant.[61] The absence of matrix swelling and dissolution was observable also during the drug release studies.

3. CONCLUSION

Polyurea (PUA) and poly(isocyanurate-urethane) (PIR-PUR) aerogels are prepared easily in a single step, and they are nontoxic, biocompatible, and biodegradable. Due to these reasons, they were investigated as drug delivery systems. A detailed study was conducted alongside, by taking advantage of their rich nanomorphologies, to investigate the effect of the morphology of these aerogels on their drug-loading and release profiles. It was found that the equilibrium drug-loading capacities of samples with approximately the same porosities and surface areas were similar to one another; furthermore, morphologies with larger surface areas (K = 1.2−1.6) tend to give higher drug-loading capacities compared to those with lower surface areas (K = 1.7−2.2). Comparing all morphologies studied, we found that slow drug release is associated with morphologies with curved and cage-like pore structures (K = 1.2 and 1.3) presumably because they create a longer nonlinear diffusion pathway for the release of loaded drugs, while morphologies with short linear diffusion pathways (K = 1.5 and 2.2) release drugs quickly. Drug release from hierarchical porous nanostructures is also slow and in a stepwise fashion, since drugs on the surfaces of the mesopores are buried underneath and are released more slowly compared to more loosely held drugs on the surfaces of the outer macropores. Also, drugs loaded onto surfaces with higher energy, for example, on highly curved nanofibers, are prone to a faster release due to their higher degree of freedom compared to drugs sitting on the surfaces of "flatter" microparticles. By studying the release kinetics of each morphology, we found that morphologies with varying ratios of particles and fibers (K = 1.6−2.0) are more useful for sustained-release technologies compared to their corresponding morphologies. It was also observed that caterpillar-like assemblies of different aspect ratios (K = 1.2 and 1.3) are more useful for extended-release formulations. Furthermore, aerogels with bicontinuous morphology or its resemblance (K = 1.5 and 2.2) are more suitable for immediate-release formulations compared to the remaining morphologies, and last, nanofibrous PUA aerogels (K = 1.6) are more suitable for controlled-release formulations.

Since similar results were obtained from testing our hypothesis with two distinct drugs, it is envisaged that the delivery of other drugs will also be significantly influenced by the morphology or the K-index of the aerogel drug carrier. We suspect that this specific K-index scale is unique to polyurea. An analogous K-index can be developed for other systems too, but due to our rather broad experience with aerogels, we are not aware of a system that will display as a broad spectrum of nanostructures as polyurea.

In summary, the significance of this work is that the drug-loading and release profiles of aerogels can be predicted based on their nanomorphologies. Conversely, the drug-carrier properties of aerogels can be controlled by tuning their morphologies. Overall, aliphatic polyurea and PIR-PUR aerogels are potentially useful drug carriers due to their rich morphologies in combination with their known biocompatibility.

4. EXPERIMENTAL SECTION

4.1. Materials. All reagents and solvents were used without further purification. Desmodur N3300A was donated by Covestro LLC, Pittsburgh, PA. Triethylamine (99% pure) was purchased from Acros-Organics and was distilled before use. Anhydrous acetonitrile (ACN), anhydrous dimethylformamide (DMF), triethylene glycol (TEG), dibutyltin dilaurate (DBTDL), and anhydrous cupric chloride ($CuCl_2$) were purchased from Sigma-Aldrich Co., and were used without further purification. Siphon-grade CO_2, and N_2 (99.999%) were purchased from Air Gas Co. (St. Louis, MO).

4.2. Preparation of PUA and PIR-PUR Aerogels. *4.2.1. Synthesis of PUA Aerogels.* PUA aerogels used in this study were synthesized following reported protocols.[13] In a typical process, triethylamine (Et_3N) was used to catalyze the reaction of 1,3,5-tris(6-isocyanatohexyl)-1,3,5-triazinane-2,4,6-trione (ISO) with water (Scheme S1a) to yield polyurea aerogels with different morphologies. The amounts of monomer and reagents used are indicated in Table S1. Wet gels obtained were dried into aerogels using supercritical fluid CO_2 technology following a process described in Section 4.3.

4.2.2. Synthesis of Flexible PIR-PUR Aerogels. PIR-PUR aerogels of this study were synthesized using reported procedures.[14] All sols were formulated at room temperature using anhydrous acetonitrile as the solvent (Scheme S1b and Table S2). The weight percent of both

https://doi.org/10.1021/acsapm.4c01765
ACS Appl. Polym. Mater. 2024, 6, 10655−10668

monomers (Desmodur N3300A and triethylene glycol (TEG)) was set at 20% w/w, and the mole ratio of Desmodur N3300A to TEG was set at 2:3. The concentration of the reference catalyst, dibutyltin dilaurate (DBTDL), was set at 1× which corresponds to 1/120 × the moles of Desmodur N3300A. The mole ratio 1/120× was chosen since it gave a reasonable gelation time (~30 min for monomers set at 20% w/w). DBTDL was replaced with an anhydrous metal salt ($CuCl_2$), and the concentration at 1× was further diluted to obtain different multiples (e.g., 1×, 1/8×, and 1/20×) of a reference concentration of dibutyltin dilaurate (DBTDL) (designated as 1×).

To prepare a $CuCl_2$ solution with an approximately same concentration as that of DBTDL (i.e., $CuCl_2$-1× sol), anhydrous $CuCl_2$ salt solutions at concentrations (1×, 1/8× and 1/20×) were prepared in a glovebox using anhydrous acetonitrile as the solvent.

In making the PIR-PUR sol, Desmodur N3300A (2.520 g, 5.00 mmol) was dissolved in 8.55 mL of anhydrous acetonitrile: meanwhile, TEG (1.125 g, 7.50 mmol) was weighed directly in a 50 mL three-neck round-bottom flask and was dissolved under N_2 with 9.50 mL of anhydrous acetonitrile at 23 °C. Then, 500 μL of the stock $CuCl_2$ solution was added to the TEG solution. The mixture was stirred for 1 min, and the isocyanate solution was added. The resulting sol was stirred for another minute and was poured into plastic syringes used as molds. The molds were covered with Parafilm TM and were stored at room temperature for gelation and aging. The gelation time varied from about 1 min to around 24 h, depending on the concentration of $CuCl_2$. Material properties of the resulting aerogels are presented in Table S3. The aging time was kept at about 16 h for all samples. This procedure was repeated several times by changing only the volume of the $CuCl_2$ stock solution that was mixed with the TEG solution, which in turn was always made with 10 mL of anhydrous acetonitrile minus the volume of the $CuCl_2$ stock catalyst solution that was transferred into it, so that the total volume of the TEG/$CuCl_2$ solution was always equal to 10 mL. After aging, the wet gels were removed from their molds and washed twice with acetonitrile and then with acetone six times. Finally, the washed wet gels were dried with supercritical fluid (SCF) CO_2 as described in the next section. The obtained aerogels were identified with their relative concentrations (1×), (1/8×), and (1/20×) like their corresponding sols.

4.3. Methods. *4.3.1. Drying Wet Gels into Aerogels.* The aerogels were obtained by drying wet gels in an autoclave (SPIDRY Jumbo Supercritical Point Dryer, SPI Supplies, Inc., West Chester, PA). The wet gels were immersed in acetone solution in a boat, which was supplied with the autoclave. The boat was then loaded to the autoclave which has been kept at 14 °C. After closing the autoclave, liquid CO_2 was siphoned into it several times alongside draining out CO_2 which was added previously. The addition and removal of CO_2 continued multiple times until all of the acetone was extracted out of the pores of the gels completely. Finally, the temperature of the autoclave was raised to 40 °C and left to stand for about an hour. Then, the supercritical fluid (SCF) CO_2 gas was vented off. The venting off process lasted for more than 5 h.

4.3.2. Characterization of Aerogels. Bulk densities (ρ_b) were calculated from the weight and physical dimensions of the samples. Skeletal densities (ρ_s) were measured using helium pycnometry with a Micromeritics AccuPyc II 1340 instrument. Scanning electron microscopy (SEM) was conducted with Au- and Pd-coated samples on a Raith e-Line scanning electron microscope to obtain topographical images of unloaded and drug-loaded aerogels. Samples were placed on the stub using a carbon dot. Thin sticky copper strips were cut and placed on the edges and top of the sample, leaving a small area uncovered for observation. Differential scanning calorimetric (DSC) thermograms were obtained for polyurea aerogel with a *K*-index of 1.2 and its drug-loaded samples using TA Instruments Q2000 DSC. Approximately 5 mg was taken from each sample and heated in sealed aluminum pans under nitrogen at a range of 0−400 °C and a rate of 10 °C/min. An empty, sealed aluminum pan was used as a reference.

The pore structure of aerogels was analyzed with N_2 sorption porosimetry at 77 K using either a Micromeritics ASAP 2020 instrument equipped with a low-pressure transducer or a TriStar II 3020 version 3.02 surface area and porosity analyzer. For each analysis, samples were first degassed for 24 h under vacuum at 80 °C. Total surface areas σ were determined via the Brunauer−Emmett−Teller (BET) method from the medium-pressure N_2 sorption isotherms. Pore size distributions for pores in the mesopore and low macropore range were obtained using the BJH method applied on the desorption branch of the medium-pressure N_2 sorption data (up to 1 bar, i.e., as $P/P_0 \rightarrow 1$). X-ray photoelectron spectroscopic analysis (XPS) was carried out with a Thermo Fischer Scientific Nexsa X-ray photoelectron spectrometer system. Samples were mixed and ground together with Au powder (5% w/w) as an internal reference.

4.3.3. Drug-Loading Procedure and Quantification. All aerogels were loaded with drugs using a previously described procedure,[23] and drug-loading amounts were determined (Scheme S3) using a previously prepared calibration curve (Figure S3). In a typical procedure, loading of aerogels with paracetamol and 5-FU was carried out by placing monoliths in vials containing saturated ethanol/water (50/50) solutions of the drugs. The volume of each drug solution was always 5× the volume of the aerogel. The vials were mildly agitated on an orbital shaker periodically for 24 h. The aerogels were carefully removed from the loading solutions and briefly dipped in a fresh solvent to remove excess loosely bound surface adsorbed drug. Drug-loaded aerogels were then dried in a vacuum oven at ambient temperature until a constant mass was obtained (~3 days). The amount of drug loaded onto the aerogels was determined gravimetrically using eq 3. Then, the absorbance of the supernatant drug solutions was measured (5-FU (λ_{max} = 265 nm), paracetamol (λ_{max} = 245 nm)) and used to determine the equilibrium drug-loading amounts following eq 2.

4.3.4. Estimation of the Maximum Drug-Loading Capacity and Loading Mechanism. Different concentrations of the drugs were loaded to equivalent mass of the aerogels (~0.5 g), and their maximum drug-loading capacities and mechanism were determined by fitting the data to the Langmuir and Freundlich models (Scheme S3). The Langmuir and Freundlich equations are presented in eqs 4 and 5, respectively.[62] The parameters, Q_m and b (Langmuir model) and K_f and $1/n$ (Freundlich model), were varied until a minimum fitting error was obtained before using them for analysis.

4.3.5. Drug Release. In a typical process, a certain amount of the drug-loaded aerogel (~0.5 g) was weighed. The sample was then mixed with 30 mL of PBS buffer (pH 7.4) and agitated on an orbital shaker for 24 h at 80 rpm. At specified time intervals (0.5, 1, 3, 6, 12, 24, 48, and 72 h), 4 mL of supernatant was carried into prelabeled Eppendorf tubes and replaced with equal amounts of fresh solvent. The absorbance of samples was read with a UV spectrophotometer at a certain wavelength (5-FU (λ_{max} = 265 nm), paracetamol (λ_{max} = 245 nm)). A standard curve plotted for this purpose (Figure S3) was used to determine the amount of drug released at each time point, and the cumulative percent of drug released at each time point is calculated using eq 11[63]

$$\text{Cumulative release} = ((C_1V_1 + C_2V_1 + \ldots + C_{n-1}V_1) + C_nV_2)/M_d \times 100\% \quad (11)$$

where C_n is the 5-FU concentration at each time, V_1 is the volume taken out at each time, and V_2 is the volume of the solution. Each experiment was repeated three times, and the average value was taken as the experimental data.

Finally, a plot of cumulative percent drug release versus time was obtained and fitted with four mathematical models, the zero-order (eq 7), first-order (eq 8), Higuchi (eq 9), and Korsmeyer−Peppas models (eq 10), to reveal the relevant release mechanism.

■ ASSOCIATED CONTENT

Supporting Information

The Supporting Information is available free of charge at https://pubs.acs.org/doi/10.1021/acsapm.4c01765.

https://doi.org/10.1021/acsapm.4c01765
ACS Appl. Polym. Mater. 2024, 6, 10655−10668

Appendix I (preparation of polyurea (PUA) and polyisocyanurate-urethane (PIR-PUR) aerogels; Appendix II (formulations of PUA and PIR-PUR aerogels of this study); Appendix III (material properties of PUA and PIR-PUR aerogels); Appendix IV (quantification of drug loading and release in PUA and PIR-PUR aerogels); Appendix V (determination of drug release profiles in PUA and PIR-PUR aerogels) (PDF)

AUTHOR INFORMATION

Corresponding Author

Chariklia Sotiriou-Leventis − *Department of Chemistry, Missouri S&T, Rolla, Missouri 65409, United States;* orcid.org/0000-0003-3283-8257; Email: cslevent@mst.edu

Authors

Stephen Y. Owusu − *Department of Chemistry, Missouri S&T, Rolla, Missouri 65409, United States;* orcid.org/0000-0002-5251-4287

A. B. M. Shaheen Ud Doulah − *Department of Chemistry, Missouri S&T, Rolla, Missouri 65409, United States;* orcid.org/0000-0002-5413-0762

Vaibhav A. Edlabadkar − *Department of Chemistry, Missouri S&T, Rolla, Missouri 65409, United States;* orcid.org/0000-0001-5763-7318

Kamden J. George − *Department of Chemistry, Missouri S&T, Rolla, Missouri 65409, United States*

Complete contact information is available at: https://pubs.acs.org/10.1021/acsapm.4c01765

Notes

The authors declare no competing financial interest.

ACKNOWLEDGMENTS

We thank the NSF for financial support under award number CMMI-1530603 (subcontract to MS&T from Tufts University).

REFERENCES

(1) Torchilin, V. P. Multifunctional Nanocarriers. *Adv. Drug Delivery Rev.* **2006**, *58*, 1532−1555.

(2) Sabatelle, R. C.; Liu, R.; Hung, Y. P.; Bressler, E.; Neal, E. J.; Martin, A.; Ekladious, I.; Grinstaff, M. W.; Colson, Y. L. Ultra-high drug loading improves nanoparticle efficacy against peritoneal mesothelioma. *Biomaterials* **2022**, *285*, 121534.

(3) Ghosh, P.; Patwari, J.; Dasgupta, S. Complexation with Human Serum Albumin Facilitates Sustained Release of Morin from Polylactic-Co-Glycolic Acid Nanoparticles. *J. Phys. Chem. B* **2017**, *121*, 1758−1770.

(4) Saini, K.; Prabhuraj, R. S.; Bandyopadhyaya, R. Development of mesoporous silica nanoparticles of tunable pore diameter for superior Gemcitabine drug delivery in pancreatic cancer cells. *J. Nanosci. Nanotechnol.* **2020**, *20*, 3084−3096.

(5) López-Iglesias, C.; Casielles, A. M.; Altay, A.; Bettini, R.; Alvarez-Lorenzo, C.; García-González, C. A. From the Printer to the Lungs: Inkjet-Printed Aerogel Particles for Pulmonary Delivery. *Chem. Eng. J.* **2019**, *357*, 559−566.

(6) Xie, H.; He, Z.; Liu, Y.; Zhao, C.; Guo, B.; Zhu, C.; Xu, J. Efficient Antibacterial Agent Delivery by Mesoporous Silica Aerogel. *ACS Omega* **2022**, *7*, 7638−7647.

(7) García-González, C. A.; Budtova, T.; Durães, L.; Erkey, C.; Del Gaudio, P.; Gurikov, P.; Koebel, M.; Liebner, F.; Neagu, M.; Smirnova, I. An Opinion Paper on Aerogels for Biomedical and Environmental Applications. *Molecules* **2019**, *24*, 1815.

(8) Qian, K. K.; Bogner, R. H. Application of mesoporous silicon dioxide and silicate in oral amorphous drug delivery systems. *J. Pharm. Sci.* **2012**, *101*, 444−463.

(9) Farzan, M.; Roth, R.; Schoelkopf, J.; Huwyler, J.; Puchkov, M. The processes behind drug loading and release in porous drug delivery systems. *Eur. J. Pharm. Biopharm.* **2023**, *189*, 133−151.

(10) Horcajada, P.; Rámila, A.; Pérez-Pariente, J.; Vallet-Regı, M. Influence of pore size of MCM-41 matrices on drug delivery rate. *Microporous Mesoporous Mater.* **2004**, *68*, 105−109.

(11) Leventis, N.; Sadekar, A.; Chandrasekaran, N.; Sotiriou-Leventis, C. Click Synthesis of Monolithic Silicon Carbide Aerogels from Polyacrylonitrile-Crosslinked 3D Silica Networks. *Chem. Mater.* **2010**, *22*, 2790−2803.

(12) Leventis, N. Polyurea Aerogels: Synthesis, Material Properties, and Applications. *Polymers* **2022**, *14*, 969−1015.

(13) Taghvaee, T.; Donthula, S.; Rewatkar, P. M.; Far, H. M.; Sotiriou-Leventis, C.; Leventis, N. *K*-Index: A Descriptor, Predictor, and Correlator of Complex Nanomorphology to Other Material Properties. *ACS Nano* **2019**, *13*, 3677−3690.

(14) Shaheen ud Doulah, A. B. M.; Mandal, C.; Far, H. M.; Edlabadkar, V. A.; Soni, R. U.; Owusu, S. Y.; Leventis, N.; Sotiriou-Leventis, C. Using Catalysis to Control the Morphology and Stiffness of Shape Memory Poly(isocyanurate−urethane) (PIR−PUR) Aerogels. *ACS Appl. Polym. Mater.* **2023**, *5*, 6851−6863.

(15) Ridolfo, R.; Tavakoli, S.; Junnuthula, V.; Williams, D. S.; Urtti, A.; van Hest, J. C. M. Exploring the Impact of Morphology on the Properties of Biodegradable Nanoparticles and Their Diffusion in Complex Biological Medium. *Biomacromolecules* **2021**, *22*, 126−133.

(16) Wang, L.-l.; Tian, C.-y.; Feng, L.-n.; Wang, X.-f.; Hou, X.-r. Effect of Morphology on the Drug Sustained-Release Performance of HA/*β*-TCP Composite. *ChemistrySelect* **2022**, *7*, No. e202202341.

(17) Korsmeyer, R. W.; Peppas, N. A. Effect of the morphology of hydrophilic polymeric matrices on the diffusion and release of water-soluble drugs. *J. Membr. Sci.* **1981**, *9*, 211−227.

(18) Lim, C.; Ramsey, J. D.; Hwang, D.; Teixeira, S. C. M.; Poon, C.-D.; Strauss, J. D.; Rosen, E. P.; Sokolsky-Papkov, M.; Kabanov, A. V. Drug-Dependent Morphological Transitions in Spherical and Worm-Like Polymeric Micelles Define Stability and Pharmacological Performance of Micellar Drugs. *Small* **2022**, *18*, 2103552.

(19) Howard, G. T. Biodegradation of polyurethane: A review. *Int. Biodeterior. Biodegrad.* **2002**, *49*, 245−252.

(20) Rocas, P.; Cusco, C.; Rocas, J.; Albericio, F. On the Importance of Polyurethane and Polyurea Nanosystems for Future Drug Delivery. *Curr. Drug Delivery* **2018**, *15*, 37−43.

(21) Sabri, F.; Boughter, J. D. J.; Gerth, D.; Skalli, O.; Phung, T. C.; Tamula, G. R.; Leventis, N. Histological evaluation of the biocompatibility of polyurea crosslinked silica aerogel implants in a rat model: A pilot study. *PLoS One* **2012**, *7*, No. e50686.

(22) García-González, C. A.; Sosnik, A.; Kalmár, J.; De Marco, L.; Erkey, C.; Concheiro, A.; Alvarez-Lorenzo, C. Aerogels in drug delivery: From design to application. *J. Controlled Release* **2021**, *332*, 40−63.

(23) Bang, A.; Sadekar, A. G.; Buback, C.; Curtin, B.; Acar, S.; Kolasinac, D.; Yin, W.; Rubenstein, D. A.; Lu, H.; Leventis, N. Evaluation of Dysprosia Aerogels as Drug Delivery Systems: A Comparative Study with Random and Ordered Mesoporous Silicas. *ACS Appl. Mater. Interfaces* **2014**, *6*, 4891−4902.

(24) Zhang, N.; Yin, Y.; Xu, S. J.; Chen, W. S. 5-Fluorouracil: Mechanisms of resistance and reversal strategies. *Molecules* **2008**, *13*, 1551−1569.

(25) Feng, S.; Nie, L.; Zou, P.; Suo, J. Effects of drug and polymer molecular weight on drug release from PLGA-mPEG microspheres. *J. Appl. Polym. Sci.*, **2015**, *132*, .

(26) Darkwah, E. K.; K. Acquah, C.; Lambon, P. S.; Ameko, D. K.; Akanji, O.; K. Ayim, J. S. Simultaneous Quantification of Acetaminophen, Caffeine, and Ibuprofen in Fixed Dose Combination

Drug Using HPLC With UV Detection. *J. Adv. Med. Pharm. Sci.* **2019**, *20*, 1−19.
(27) Zheng, X.; Feng, S.; Wang, X.; Shi, Z.; Mao, Y.; Zhao, Q.; Wang, S. MSNCs and MgO-MSNCs as drug delivery systems to control the adsorption kinetics and release rate of indomethacin. *Asian J. Pharm. Sci.* **2019**, *14*, 275−286.
(28) Elmas, A.; Akyüz, G.; Bergal, A.; Andaç, M.; Andaç, Ö. Mathematical Modelling of Drug Release. *Res. Eng. Struct. Mater.* **2020**, *6*, 327−350.
(29) Adom, S. *Effects of pH on adsorption of copper (II) onto ground peanut hulls*. M.S. Dissertation, Western Carolina University: Cullowhee, NC 2020.
(30) García-González, C. A.; Alnaief, M.; Smirnova, I. Polysaccharide-based aerogels—Promising biodegradable carriers for drug delivery systems. *Carbohydr. Polym.* **2011**, *86*, 1425−1438.
(31) Jiang, S.; Shi, R.; Cheng, H.; Zhang, C.; Zhao, F. Synthesis of polyurea from 1,6-hexanediamine with CO_2 through a two-step polymerization. *Green Energy Environ.* **2017**, *2*, 370−376.
(32) Şanli, O.; Kahraman, A.; Solak, E. K.; Olukman, M. Preparation of magnetite-chitosan/methylcellulose nanospheres by entrapment and adsorption techniques for targeting the anti-cancer drug 5-fluorouracil. *Artif. Cells, Nanomed., Biotechnol.* **2016**, *44*, 950−959.
(33) Michael, A. M.; Rajendar, R. M.; McHugh, M. A. Silk fibroin aerogels for drug delivery applications. *J. Supercrit. Fluids* **2014**, *91*, 84−89.
(34) Rokhade, A. P.; Kulkarni, P. V.; Mallikarjuna, N. N.; Aminabhavi, T. M. Preparation and characterization of novel semi-interpenetrating polymer network hydrogel microspheres of chitosan and hydroxypropyl cellulose for controlled release of chlorothiazide. *J. Microencapsulation* **2009**, *26*, 27−36.
(35) Zalac, S.; Khan, M. Z. I.; Gabelica, M. V.; Tudja, M.; Mestrović, E.; Romih, M. Paracetamol-Propyphenazone Interaction and Formulation Difficulties Associated with Eutectic Formation in Combination Solid Dosage Forms. *Chem. Pharm. Bull.* **1999**, *47*, 302−307.
(36) Edlabadkar, V. A.; Soni, R. U.; Shaheen ud Doulah, A. B. M.; Owusu, S. Y.; Hackett, S.; Bartels, J. M.; Leventis, N.; Sotiriou-Leventis, C. CO_2 Uptake by Microporous Carbon Aerogels Derived from Polybenzoxazine and Analogous All-Nitrogen Polybenzodiazine Aerogels. *Chem. Mater.* **2024**, *36*, 1172−1187.
(37) Ganguli, A. K.; Kunde, G. B.; Raza, W.; Kumar, S.; Yadav, P. Assessment of Performance of Photocatalytic Nanostructured Materials with Varied Morphology Based on Reaction Conditions. *Molecules* **2022**, *27*, 7778.
(38) Falahati, M. T.; Ghoreishi, S. M. Preparation of Balangu (Lallemantia royleana) seed mucilage aerogels loaded with paracetamol: Evaluation of drug loading via response surface methodology. *J. Supercrit. Fluids* **2019**, *150*, 1−10.
(39) Zhao, J.; Lu, C.; He, X.; Zhang, X.; Zhang, W.; Zhang, X. Polyethylenimine-Grafted Cellulose Nanofibril Aerogels as Versatile Vehicles for Drug Delivery. *ACS Appl. Mater. Interfaces* **2015**, *7*, 2607−2615.
(40) Wang, C.; Okubayashi, S. 3D Aerogel of Cellulose Triacetate with Supercritical Antisolvent Process for Drug Delivery. *J. Supercrit. Fluids* **2019**, *148*, 33−41.
(41) Sang, Y.; Miao, P.; Chen, T.; Zhao, Y.; Chen, L.; Tian, Y.; Han, X.; Gao, J. Fabrication and Evaluation of Graphene Oxide/Hydroxypropyl Cellulose/Chitosan Hybrid Aerogel for 5-Fluorouracil Release. *Gels* **2022**, *8*, 649.
(42) Chung, H.-K.; Kim, W.-H.; Park, J.; Cho, J.; Jeong, T.-Y.; Park, P.-K. Application of Langmuir and Freundlich isotherms to predict adsorbate removal efficiency or required amount of adsorbent. *J. Ind. Eng. Chem.* **2015**, *28*, 241−246.
(43) Wang, J.; Guo, X. Adsorption Isotherm Models: Classification, Physical Meaning, Application and Solving Method. *Chemosphere* **2020**, *258*, 127279.
(44) Qu, F.; Zhu, G.; Huang, S.; Li, S.; Sun, J.; Zhang, D.; Qiu, S. Controlled release of Captopril by regulating the pore size and morphology of ordered mesoporous silica. *Microporous Mesoporous Mater.* **2006**, *92*, 1−9.
(45) de Sá, A.; Abreu, A. S.; Moura, I.; Machado, A. V. Polymeric materials for metal sorption from hydric resources. *Water Purif.* **2017**, 289−322.
(46) Perdigoto, M. L. N.; Martins, R. C.; Rocha, N.; Quina, M. J.; Gando-Ferreira, L.; Patrício, R.; Durães, L. Application of hydrophobic silica-based aerogels and xerogels for removal of toxic organic compounds from aqueous solutions. *J. Colloid Interface Sci.* **2012**, *380*, 134−140.
(47) Mohammadi, A.; Moghaddas, J. Mesoporous tablet-shaped potato starch aerogels for loading and release of the poorly water-soluble drug celecoxib. *Chin. J. Chem. Eng.* **2020**, *28*, 1778−1787.
(48) Dereka, B.; Yu, Q.; Lewis, N. H. C.; Carpenter, W. B.; Bowman, J. M.; Tokmakoff, A. Crossover from hydrogen to chemical bonding. *Science* **2021**, *371*, 160−164.
(49) Andersson, J.; Rosenholm, J.; Areva, S.; Lindén, M. Influences of Material Characteristics on Ibuprofen Drug Loading and Release Profiles from Ordered Micro- and Mesoporous Silica Matrices. *Chem. Mater.* **2004**, *16*, 4160−4167.
(50) Farzan, M.; Roth, R.; Schoelkopf, J.; Huwyler, J.; Puchkov, M. The processes behind drug loading and release in porous drug delivery systems. *Eur. J. Pharmacol.* **2023**, *189*, 133−151.
(51) Heikkila, T.; Salonen, J.; Tuura, J.; Hamdy, M. S.; Mul, G.; Kumar, N.; Salmi, T.; Murzin, D. Y.; Laitinen, L.; Kaukonen, A. M.; et al. Mesoporous silica material TUD-1 as a drug delivery system. *Int. J. Pharm.* **2007**, *331*, 133−138.
(52) Aerts, C. A.; Verraedt, E.; Mellaerts, R.; Depla, A.; Augustijns, P.; Van Humbeeck, J.; Van den Mooter, G.; Martens, J. A. Tunability of Pore Diameter and Particle Size of Amorphous Microporous Silica for Diffusive Controlled Release of Drug Compounds. *J. Phys. Chem. C* **2007**, *111*, 13404−13409.
(53) Veber, D. F.; Johnson, S. R.; Cheng, H. Y.; Smith, B. R.; Ward, K. W.; Kopple, K. D. Molecular properties that influence the oral bioavailability of drug candidates. *J. Med. Chem.* **2002**, *45*, 2615−2623.
(54) Bard, A. J.; Faulkner, L. J. *Electrochemical Methods, Fundamentals and Applications*. 2nd ed.; Wiley: New York, 2000, pp 864.
(55) Chen, W.; Palazzo, A.; Hennink, W. E.; Kok, R. J. Effect of Particle Size on Drug Loading and Release Kinetics of Gefitinib-Loaded PLGA Microspheres. *Mol. Pharm.* **2017**, *14*, 459−467.
(56) Mohite, D. P.; Larimore, Z. J.; Lu, H.; Mang, J. T.; Sotiriou-Leventis, C.; Leventis, N. Monolithic Hierarchical Fractal Assemblies of Silica Nanoparticles Cross-Linked with Polynorbornene via ROMP: A Structure−Property Correlation from Molecular to Bulk through Nano. *Chem. Mater.* **2012**, *24*, 3434−3448.
(57) Adepu, S.; Ramakrishna, S. Controlled Drug Delivery Systems: Current Status and Future Directions. *Molecules* **2021**, *26*, 5905.
(58) Jantzen, G. M.; Robinson, J. R. Sustained and Controlled-release Drug Delivery Systems. *Modern Pharmaceutics, Fourth Edition Revised and Expanded*, CRC Press, 2002, pp. 43.
(59) Pooresmaeil, M.; Asl, E. A.; Namazi, H. Simple fabrication of biocompatible chitosan/graphene oxide microspheres for pH-controlled amoxicillin delivery. *Eur. Polym. J.* **2021**, *159*, 110706.
(60) Li, J.; Wang, Y. J.; Zhang, L.; Xu, Z.; Dai, H.; Wu, W. Nanocellulose/Gelatin Composite Cryogels for Controlled Drug Release. *ACS Sustainable Chem. Eng.* **2019**, *7*, 6381−6389.
(61) Dash, S.; Murthy, P. N.; Nath, L.; Chowdhury, P. Kinetic Modeling on Drug Release from Controlled Drug Delivery Systems. *Acta Polym. Pharm.* **2010**, *67*, 217−223.
(62) Khayyun, T. S.; Mseer, A. H. Comparison of the experimental results with the Langmuir and Freundlich models for copper removal on limestone adsorbent. *Appl. Water Sci.* **2019**, *9*, 170.
(63) Liu, Z.; Zhang, S.; Gao, C.; Meng, X.; Wang, S.; Kong, F. Temperature/pH-Responsive Carboxymethyl Cellulose/Poly (*N*-isopropyl acrylamide) Interpenetrating Polymer Network Aerogels for Drug Delivery Systems. *Polymers* **2022**, *14*, 1578.

https://doi.org/10.1021/acsapm.4c01765
ACS Appl. Polym. Mater. 2024, 6, 10655−10668